AFRL-MN-EG-TP-2007-7406

EQUATION OF STATE OF ALUMINUM-IRON OXIDE – EPOXY COMPOSITE

Jennifer L. Jordan (AFRL/MNME)
Jason R. Foley (AFRL/MNMF)
Air Force Research Laboratory
Munitions Directorate
Eglin AFB, FL 32542-6810

Richard D. Dick
Shock Unlimited
Albuquerque, NM 87114

Louis Ferranti
Naresh N. Thadhani
David L. McDowell
School of Materials Science & Eng.
Georgia Institute of Technology
Atlanta, GA 30332

Ryan A. Austin
School of Mechanical Eng.
Georgia Institute of Technology
Atlanta, GA 30332

David J. Benson
Dept. of Mechanical & Aerospace Eng.
University of California @ San Diego
La Jolla, CA 92093

JULY 2007

JOURNAL ARTICLE

AIR FORCE RESEARCH LABORATORY, MUNITIONS DIRECTORATE

■ **Air Force Materiel Command** ■ **United States Air Force** ■ **Eglin Air Force Base**

REPORT DOCUMENTATION PAGE

Form Approved
OMB No. 0704-0188

PLEASE DO NOT RETURN YOUR FORM TO THE ABOVE ADDRESS.

1. REPORT DATE *(DD-MM-YYYY)*	2. REPORT TYPE	3. DATES COVERED *(From - To)*
XX-07-2007	JOURNAL ARTICLE	

4. TITLE AND SUBTITLE

EQUATION OF STATE OF ALUMINUM-IRON OXIDE – EPOXY COMPOSITE

5a. CONTRACT NUMBER
F08630-03-C-0001

5b. GRANT NUMBER

5c. PROGRAM ELEMENT NUMBER
62602F

6. AUTHOR(S)

1. Jennifer L. Jordan (MNME), Jason R. Foley (MNMF)
2. Richard D. Dick
3. Louis Ferranti, Naresh N. Thadhani, David McDowell
4. Ryan Austin
5. David Benson

5d. PROJECT NUMBER
2502

5e. TASK NUMBER
10

5f. WORK UNIT NUMBER
51

7. PERFORMING ORGANIZATION NAME(S) AND ADDRESS(ES)

1. Air Force Research Lab., Munitions Directorate SEE COVER PAGE FOR ADDRESSES
2. Shock Unlimited
3. Georgia Institute of Technology (School of Material Science & Eng.)
4. Georgia Institute of Technology (School of Mechanical Eng.)
5. University of CA @ San Diego (Dept. of Mechanical & Aerospace Eng.)

8. PERFORMING ORGANIZATION REPORT NUMBER
AFRL-MN-EG-TP-2007-7406

9. SPONSORING/MONITORING AGENCY NAME(S) AND ADDRESS(ES)

Air Force Research Laboratory
Munitions Directorate
AFRL/MNME
Eglin AFB, FL 32542-6810

10. SPONSOR/MONITOR'S ACRONYM(S)
AFRL-MN-EG

11. SPONSOR/MONITOR'S REPORT NUMBER(S)
SAME AS BLOCK 8

12. DISTRIBUTION/AVAILABILITY STATEMENT

DISTRIBUTION A: Approved for public release; distribution unlimited.
Approval Confirmation #AAC/PA 01-11-07-012; dated 11 January 2007.

13. SUPPLEMENTARY NOTES

 [DOI: 10.1063/1.2719272] This paper is published in The Journal of Applied Physics, 2007 Vol. 101, Issue 9, 093520.

14. ABSTRACT

ABSTRACT: We report on the measurements of the shock equation of state (Hugoniot) of an Al/Fe2O3/epoxy composite, prepared by epoxy cast curing of powder mixtures. Explosive loading, with Baratol, trinitrotoluene (TNT), and Octol, was used for performing experiments at higher pressures, in which case shock velocities were measured in the samples and aluminum, copper, or polymethyl methacrylate (PMMA) donor material, using piezoelectric pins. The explosive loading of the metal donors (aluminum and copper) will be discussed. Gas gun experiments provide complementary lower pressure data in which piezoelectric polyvinylidene fluoride (PVF) stress gauges were used to measure the input and propagated stress wave profiles in the sample and the corresponding shock propagation velocity. The results of the Hugoniot equation of state are compared with mesoscale finite-element simulations, which show good agreement.

15. SUBJECT TERMS

16. SECURITY CLASSIFICATION OF:			17. LIMITATION OF ABSTRACT	18. NUMBER OF PAGES	19a. NAME OF RESPONSIBLE PERSON
a. REPORT	b. ABSTRACT	c. THIS PAGE			Jennifer L. Jordan
UNCLASSIFIED	UNCLASSIFIED	UNCLASSIFIED	SAR	11	19b. TELEPHONE NUMBER *(Include area code)*

Equation of state of aluminum-iron oxide-epoxy composite

Jennifer L. Jordan[a)]
Air Force Research Laboratory, 2306 Perimeter Road, Eglin AFB, Florida 32542

Louis Ferranti
School of Materials Science and Engineering, Georgia Institute of Technology, Atlanta, Georgia 30332-0254

Ryan A. Austin
G.W. Woodruff School of Mechanical Engineering, Georgia Institute of Technology, Atlanta, Georgia 30332-0405

Richard D. Dick
Shocks Unlimited, Albuquerque, New Mexico 87114

Jason R. Foley
Air Force Research Laboratory, 2306 Perimeter Road, Eglin AFB, Florida 32542

Naresh N. Thadhani and David L. McDowell
School of Materials Science and Engineering, Georgia Institute of Technology, Atlanta, Georgia 30332-0254 and G.W. Woodruff School of Mechanical Engineering, Georgia Institute of Technology, Atlanta, Georgia 30332-0405

David J. Benson
Department of Mechanical and Aerospace Engineering, University of California at San Diego, La Jolla, California 92093-0404

(Received 17 January 2007; accepted 21 February 2007; published online 11 May 2007)

We report on the measurements of the shock equation of state (Hugoniot) of an Al/Fe_2O_3/epoxy composite, prepared by epoxy cast curing of powder mixtures. Explosive loading, with Baratol, trinitrotoluene (TNT), and Octol, was used for performing experiments at higher pressures, in which case shock velocities were measured in the samples and aluminum, copper, or polymethyl methacrylate (PMMA) donor material, using piezoelectric pins. The explosive loading of the metal donors (aluminum and copper) will be discussed. Gas gun experiments provide complementary lower pressure data in which piezoelectric polyvinylidene fluoride (PVDF) stress gauges were used to measure the input and propagated stress wave profiles in the sample and the corresponding shock propagation velocity. The results of the Hugoniot equation of state are compared with mesoscale finite-element simulations, which show good agreement. © *2007 American Institute of Physics*. [DOI: 10.1063/1.2719272]

I. INTRODUCTION

Equation of state studies on epoxy-based particulate composite systems, particularly alumina-epoxy systems, have been reported in the literature,[1–3] as epoxy-based composites are becoming more widely used for structural applications because of their low densities and relatively high strengths. The properties of the composite can be tuned based on the properties and volume fraction of the particulate phase(s). Results for shock wave propagation in these composite materials show dispersive waves with no elastic precursor. In particular, Anderson, *et al.*[2] and Deas *et al.*[3] have observed that the Hugoniot data for these composite systems showed a linear relationship between pressure and particle velocity over the range of conditions investigated.

The research presented in this article focuses on equation of state measurements performed on Al and Fe_2O_3 powders cast-cured in an epoxy binder. The combination of aluminum and iron oxide has been studied as the traditional thermite reaction. The shock compression behavior of these powder mixtures was first reported by Holman *et al.*[4] While no evidence of chemical reaction was revealed in these powder mixtures at pressures less than 15 GPa, it was found that the shock compression response was dominated by the dissimilar compressibilities of the softer Al and harder Fe_2O_3 powders.

In this article, equation of state measurements are presented for aluminum and iron oxide powders in an epoxy matrix. Results over a wide range of pressures are obtained from both gas gun and explosive loading experiments. A discussion of the explosive loading of metal plates used as donor materials is also included. Finally, the experimental Hugoniot is compared with that calculated by mesoscale finite-element simulation.[5]

II. EXPERIMENTAL PROCEDURE

A. Sample preparation

Spherical aluminum powder and blocky iron oxide powder were obtained in particle sizes of approximately 2 μm for the Al and 0.3 μm for Fe_2O_3, as shown in Figs. 1(a) and

[a)]Electronic mail: jennifer.jordan@eglin.af.mil

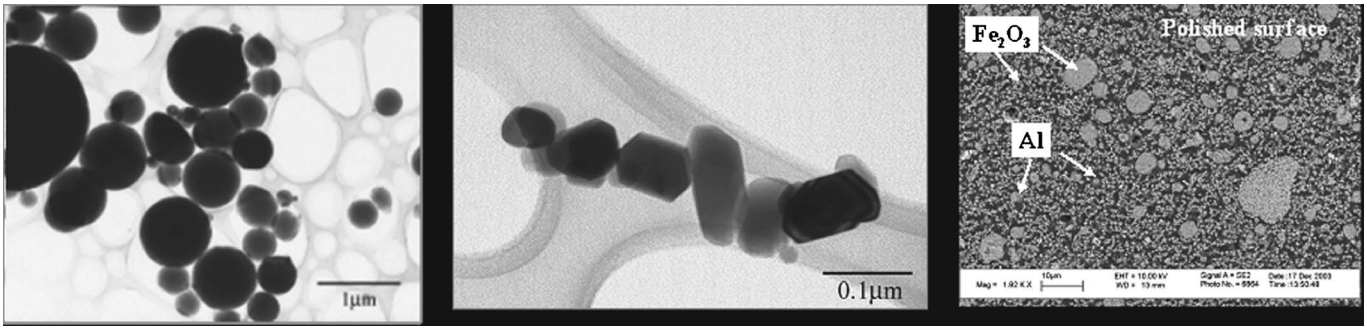

FIG. 1. Micrographs of (a) spherical aluminum powder (1–2 μm particle size); (b) blocky iron oxide powder ~0.3 μm, and (c) as-cast composite material showing Al, Fe_2O_3 agglomerates (~8 μm average size) in an epoxy matrix.

1(b), respectively. The powders were blended with Epon 826 epoxy (Hexion Specialty Chemicals) cured with diethanolamine (DEA) hardener, poured into aluminum molds, vacuum degassed at 70 °C, and cast in the form of 50 mm diameter by 125 mm long rods. Sections of ~5 mm thickness were sliced from the rod and used for performing Hugoniot measurements. The weight percents of the Al, Fe_2O_3, and epoxy were 12.63, 37.37, and 50%, respectively. Prior to performing the Hugoniot measurements the samples were characterized to determine their density, acoustic wave speed, and microstructure. Figure 1(c) shows the microstructure of a polished surface of the sample, revealing the rounded Al particles and Fe_2O_3 agglomerates (of ~8 μm average size) interspersed in an epoxy matrix.

B. Gas gun loading experiments

Four equation of state experiments, listed in Table I, were conducted at Georgia Tech using the 80 mm diameter single-stage light-gas gun at impact velocities between 500 and 950 m/s. The experiments were instrumented with Bauer piezoelectric polyvinylidene fluoride (PVDF) stress gauges[6] obtained from Ktech Corporation, Albuquerque, NM. The gauges were mounted on the front and rear surfaces of the sample (as shown in Fig. 2), which was sandwiched between a copper driver and a PMMA backer plate. An aluminum projectile with a copper flyer plate (9.5 mm nominal thickness), backed by an air gap, was used to impact a copper driver plate (6.3 mm nominal thickness). The gauge mounted between the copper driver and the sample provided an "input" stress profile, and the gauge mounted between the sample and the PMMA backer provided the "propagated" stress profile. The thicknesses of the flyer, driver, and target plates were adjusted to ensure that a steady-state shock wave propagated through the sample thickness without attenuation. The travel time between the two gauges (less the time of travel through the gauge package) was used to determine the shock wave speed in a sample of known thickness. Assuming hydrodynamic conditions and steady-state wave propagation through the sample, the measured input stress and the shock wave speed, combined with the jump conditions, were used to determine the particle velocity and pressure Hugoniot.

C. Explosive loading experiments

Twenty-five experiments, detailed in Table II and shown schematically in Fig. 3, were conducted at Eglin AFB using explosive plane wave lenses (PWL) to generate shock loading at higher pressures. In these experiments, the PWL was in contact with an explosive pad of Baratol, TNT, or Octol (12.5 or 25.4 mm thick) to generate a range of pressures in a 6061-T6 aluminum (Al), OFHC copper (Cu), or PMMA donor plate. In experiments JJH8–12, the explosive pad was 12.5 mm thick, and in the other experiments the explosive pad was 25.4 mm thick.

In explosive loading experiments, the shock wave travels from the donor to the sample. The shock velocity in the Al or Cu donor material and the sample was measured using piezoelectric pins (Dynasen CA-1135), which were placed in holes drilled into the sample at differing depths. Using the shock velocity in the donor plate and the sample, the remaining Hugoniot properties for the sample were determined using impedance matching.

In experiments JJH8–12, six piezoelectric pins were placed in the sample and the donor plate to characterize the shock velocity in both materials. In experiments JJH13–26, nine piezoelectric pins were used. Experiments JJH36–52 were designed to characterize the explosive-metal interaction [Fig. 3(b)]. In these experiments, 20 piezoelectric pins were used to get a statistical representation of the shock velocity in the metal donor in contact with the explosive.

A representative plane wave lens similar to those used in these experiments, was characterized to determine the planarity of the lens in the confined configuration of the experi-

TABLE I. Experimental details for equation of state experiments utilizing gas gun loading.

Expt. no.	Target thickness (mm)	Target density (g/cm^3)	Cu flyer thickness (mm)	Impact velocity (m/s)	Copper donor thickness (mm)
0303	3.9131±0.0053	1.7900±0.0122	9.5123±0.0025	523±27	6.2814±0.0025
0308	3.8034±0.0066	1.8645±0.0019	9.4996±0.0025	553±43	6.3017±0.0025
0311	3.8212±0.0038	1.8503±0.0082	9.5204±0.0025	714±89	6.3251±0.0051
0403	3.8735±0.0064	1.8588±0.1765	9.5148±0.0025	944±4	6.3119±0.0051

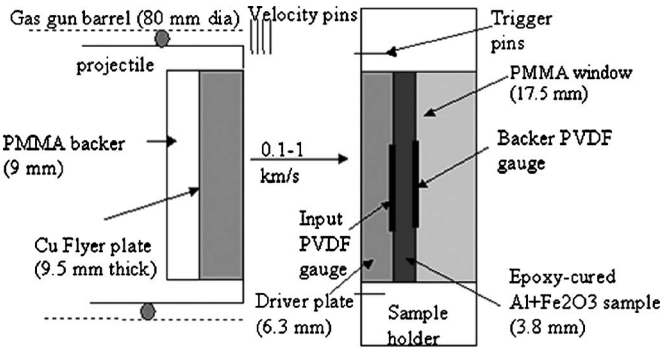

FIG. 2. Schematic of experiments performed on Al/Fe_2O_3/epoxy composites using gas gun loading showing the placement of stress gauges used to monitor input and propagated stress profiles.

ments. The streak camera record showing the breakout of the detonation wave is illustrated in the inset of Fig. 4. The breakout of the wave was digitized as a function of position and time, as shown in Fig. 4; the simultaneity of the plane wave lens breakout is ±40 ns.

III. RESULTS AND DISCUSSION

In all explosive loading experiments, the shock velocity was calculated by fitting a line to the position versus time data for all pins. The shock wave velocity (U_s) for a given sample are provided in Tables III and IV. A tilt correction was applied to the shock velocity data based on a method described by Dick.[7] In this method, the pin arrival times, t_i,

TABLE II. Experimental details for equation of state experiments utilizing explosive plane wave lens loading.

Expt. no.	Explosive	Thickness (mm)	Donor	Sample
JJH8	TNT	12.5	Al	Al/Fe_2O_3/epoxy
JJH9	TNT	12.5	PMMA/Al	Al/Fe_2O_3/epoxy
JJH10	TNT	12.5	PMMA	Al/Fe_2O_3/epoxy
JJH11	Octol	12.5	Al	Al/Fe_2O_3/epoxy
JJH12	Octol	12.5	PMMA/ Al	Al/Fe_2O_3/epoxy
JJH13	Octol	12.5	PMMA	Al/Fe_2O_3/epoxy
JJH16	Baratol	25.4	Al	Donor only
JJH42	Baratol	25.4	Al	Donor only
JJH43	Baratol	25.4	Al	Donor only
JJH25	Baratol	25.4	Cu	Al/Fe_2O_3/epoxy
JJH51	Baratol	25.4	Cu	Donor only
JJH52	Baratol	25.4	Cu	Donor only
JJH14	TNT	25.4	Al	Donor only
JJH22	TNT	25.4	Al	Donor only
JJH36	TNT	25.4	Al	Donor only
JJH37	TNT	25.4	Al	Donor only
JJH24	TNT	25.4	Cu	Al/Fe_2O_3/epoxy
JJH45	TNT	25.4	Cu	Donor only
JJH46	TNT	25.4	Cu	Donor only
JJH15	Octol	25.4	Al	Donor only
JJH39	Octol	25.4	Al	Donor only
JJH40	Octol	25.4	Al	Donor only
JJH26	Octol	25.4	Cu	Al/Fe_2O_3/epoxy
JJH48	Octol	25.4	Cu	Donor only
JJH49	Octol	25.4	Cu	Donor only

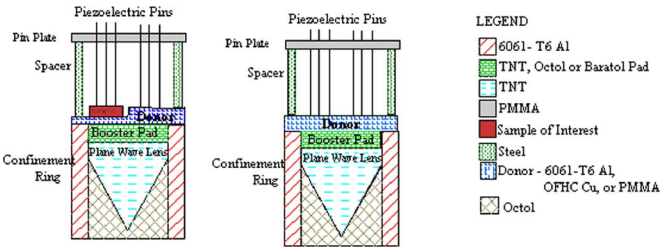

FIG. 3. (Color online) Schematic of equation of state experiments on Al/Fe_2O_3/epoxy composites using explosive loading where (a) is the configuration used for experiments JJH8–16 and 24–26 and (b) is the configuration used for JJH36–52.

the pin depths, z_i, and the pin coordinates on the surface of the donor plate, x_i andy_i, are fitted to the equation

$$t_i = P_1 + P_2 z_i + P_3 x_i + P_4 y_i, \tag{1}$$

where the subscript i indicates each pin time and corresponding pin location. The constants P_3 and P_4 are a measure of the tilt of the shock wave with respect to the plane of the pin circle. The time the pins would have discharged had there been no tilt, t_{ci}, can be represented as

$$t_{ci} = t_i - P_3 x_i - P_4 y_i = P_1 + P_2 z_i, \tag{2}$$

where P_1 is the intercept and P_2 is the slope of the corrected time, t_c. The reciprocal of this slope is the corrected shock velocity, recorded in Tables III and IV as "U_s Tilt Corr." In experiments with only one pin circle in the donor plate and one in the sample, the correction was performed to the center of the pin circle. In experiments (JJH39–52) with two pin circles, the correction was performed to the center of the explosive charge.

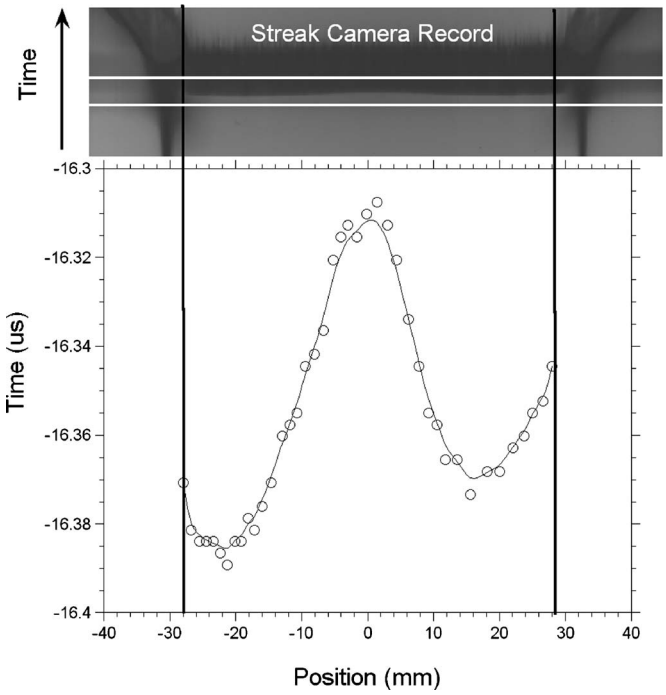

FIG. 4. Breakout of detonation wave from TNT/Octol plane wave lens as a function of position and time. The inset picture shows the original streak camera record.

TABLE III. Measured shock velocity (U_s) with calculated pressure (P) and particle velocity (U_p) in aluminum and copper donors in contact with TNT, Octol, and Baratol compared with literature values. In JJH8–12, the explosive pad was 12.5 mm thick. In all other experiments, the explosive pad was 25.4 mm thick.

Expt. no.	Explosive	Donor	U_s (mm/μs)	U_s tilt corr. (mm/μs)	U_s avg. (mm/μs)	U_s lit. (mm/μs)	P (GPa)	U_p (mm/μs)
JJH10	TNT	PMMA	5.42±0.19	5.42±0.19			12.0±0.9	1.86±0.13
JJH9	TNT	PMMA / Al	6.97±0.52	6.99±0.48			23.2±6.9	1.23±0.36
JJH8	TNT	Al	6.62±0.44	6.63±0.42			17.1±5.8	0.95±0.32
JJH13	Octol	PMMA	5.72±0.25	5.75±0.15			14.2±0.8	2.08±0.10
JJH12	Octol	PMMA/ Al	7.29±0.29	7.33±0.15			29.2±2.3	1.48±0.11
JJH11	Octol	Al	7.12±0.12	7.13±0.08			25.5±1.2	1.32±0.06
JJH16	Baratol	Al	6.73±0.67	6.99±0.40		6.7		
JJH42	Baratol	Al	6.29±0.40	6.74±0.06			21.2±2.2	1.14±0.10
JJH43	Baratol	Al	6.33±0.45	6.90±0.02	6.89±0.20			
JJH25	Baratol	Cu	4.48±0.52	4.79±0.20	4.79±0.09			
JJH51	Baratol	Cu	4.32±0.31	4.71±0.07		4.5	24.5±2.9	0.57±0.06
JJH52	Baratol	Cu	4.55±0.29	4.88±0.05				
JJH14	TNT	Al	6.30±0.49	6.39±0.39				
JJH22	TNT	Al	6.93±0.80	7.31±0.46	6.89±0.20	7.0	21.5±3.0	1.15±0.16
JJH36	TNT	Al	6.60±0.35	6.90±0.11				
JJH37	TNT	Al	6.67±0.33	6.95±0.06				
JJH24	TNT	Cu	4.93±0.12	4.95±0.03				
JJH45	TNT	Cu	4.56±0.19	4.69±0.05	4.79±0.14	4.8	24.5±4.8	0.57±0.09
JJH46	TNT	Cu	4.57±0.21	4.73±0.01				
JJH15	Octol	Al	6.66±0.64	6.81±0.50		7.8		
JJH39	Octol	Al	7.38±0.20	7.45±0.12				1.38±0.25
JJH40	Octol	Al	7.24±0.19	7.32±0.06	7.19±0.34		26.8±6.0	
JJH26	Octol	Cu	4.64±0.40	4.66±0.38				
JJH48	Octol	Cu	5.13±0.11	5.16±0.02	4.91±0.25	5.4	28.9±8.9	0.65±0.17
JJH49	Octol	Cu	4.87±0.10	4.91±0.01				

In determining the shock velocity (for both uncorrected and corrected values) the displacement data vector ($\mathbf{z}_{\text{data}}$) is a linear function of time, i.e., $\mathbf{z}(\mathbf{t})=a_1\mathbf{t}+a_2$, where a_1 and a_2 are unknown coefficients. A straightforward maximum likelihood estimator (MLE) approach is implemented[8] where the vector of error in the data (i.e., the residual),

TABLE IV. Shock velocity (U_s), pressure (P), and particle velocity (U_p) in Al/Fe_2O_3/epoxy samples from gas gun and explosive loading. The experimentally measured values are italic.

Expt. no.	Initial density (g/cm^3)	U_s (mm/μs)	U_s tilt corr. (mm/μs)	U_p (mm/μs)	P_{in} (GPa)	P_{out} (GPa)
0303	1.790±0.012	*3.17±0.01*		0.372±0.006	2.11±0.02	*1.76±0.22*
0308	1.865±0.002	*3.47±0.01*		0.364±0.004	*2.35±0.35*	
0311	1.850±0.008	*3.65±0.01*		0.499±0.004	*3.37±0.12*	*2.95±0.06*
0403	1.856±0.177	*3.92±0.01*		0.641±0.005	4.66±0.31	*3.56±0.4*
JJH25	1.850±0.027	*3.42±0.26*	3.50±0.15	0.97±0.24	6.3±1.6	
JJH26	1.850±0.027	*4.84±0.13*	4.85±0.06	0.78±0.41	7.0±3.6	
JJH24	1.850±0.027	*4.18±0.09*	4.19±0.04	1.13±0.02	8.7±0.3	
JJH8	1.850±0.027	*5.16±0.11*	5.16±0.11	1.22±0.41	11.7±3.9	
JJH9	*1.850*±0.027	*4.71±0.36*	4.77±0.26	1.63±0.49	14.4±4.4	
JJH10	1.850±0.027	*5.12±0.23*	5.14±0.18	1.57±0.11	15.0±1.2	
JJH11	1.850±0.027	*5.34±0.16*	5.35±0.13	1.71±0.08	16.9±0.9	
JJH13	1.850±0.027	*5.46±0.46*	5.46±0.46	1.76±0.12	17.7±1.9	
JJH12	1.850±0.027	*4.93±0.33*	4.96±0.27	1.96±0.16	17.9±1.8	
JJH22/23	1.850±0.027	*5.47±0.36*	5.52±0.24	11.88±0.46	19.2±4.8	

$$\mathbf{r} = \mathbf{z}(\mathbf{a},t) - \mathbf{z}_{\text{data}}, \tag{3}$$

is minimized in a least-squares sense to find the best estimate of the unknowns ($\hat{\mathbf{x}}$), i.e.,

$$\hat{\mathbf{a}} \leftarrow \text{argmin}_x(\mathbf{r}^T\boldsymbol{\Pi}_z^{-1}\mathbf{r}), \tag{4}$$

where $\boldsymbol{\Pi}_z$ is the covariance matrix of the uncertainties $\boldsymbol{\sigma}_z$ in the $z(t)$ data.[9] However, $\boldsymbol{\Pi}_\mathbf{z}$ is not known prior to the analysis, so the uncertainty in the data of length N_z is estimated from an unweighted solution of Eq. (4).[10] Here $\boldsymbol{\Pi}_z = \mathbf{I}$, such that

$$\sigma_z \approx \sqrt{\frac{\mathbf{r}^T\mathbf{r}}{N_z - 2}}, \tag{5}$$

and correspondingly

$$\boldsymbol{\Pi}_z = \sigma_z^2\mathbf{I}. \tag{6}$$

The estimate of the uncertainty in $\hat{\mathbf{x}}$ is then found by applying a *QR* decomposition to the Jacobian matrix, $\mathbf{J}$, for the displacement function with respect to the estimation parameters,[10]

$$\mathbf{J} = [\mathbf{t} \quad \mathbf{1}\,] = \mathbf{QR}, \tag{7}$$

where $\mathbf{Q}$ is unitary and $\mathbf{R}$ is upper triangular. The estimated covariance of the parameters at the best estimate is then found from

$$\boldsymbol{\Pi}_x = (\mathbf{R}^T\boldsymbol{\Pi}_z\mathbf{R})^{-1}. \tag{8}$$

Using this approach, the error and correlations in the shock velocity, both corrected and uncorrected can be determined.

For the donor materials, the remaining parameters (particle velocity, U_p, and pressure, P) can be determined based on the published Hugoniot data,[11,12] which are given by

$$U_s = 5.35 + 1.34U_p, \tag{9}$$

for 6061-T6 Al, with an initial density, $\rho_0 = 8.93$ g/cm^3, and

$$U_s = 3.94 + 1.49U_p, \tag{10}$$

for OFHC copper, with an initial density, $\rho_0 = 8.93$ g/cm^3, and

$$U_s = 2.60 + 1.52U_p, \tag{11}$$

for PMMA, with an initial density, $\rho_0 = 1.19$ g/cm^3, and the Rankine-Hugoniot jump conditions,[12] namely,

$$P = \rho_0 U_s U_p. \tag{12}$$

Equations (9)–(11) take the form $U_s = C_0 + SU_p$. Here, C_0 represents the bulk sound speed and the S represents a linear empirical dependence of the shock velocity on the particle velocity. The errors in the particle velocity and pressure are propagated according to standard quadrature estimates,

$$\Delta U_p = U_p\left(\frac{\Delta U_s}{U_s - C_0}\right), \tag{13}$$

and

$$\Delta P = P\sqrt{\left(\frac{\Delta U_s}{U_s}\right)^2 + \left(\frac{\Delta U_p}{U_p}\right)^2}. \tag{14}$$

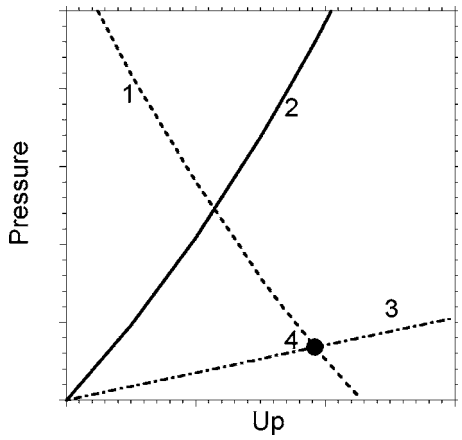

FIG. 5. Schematic of impedance matching method where line 1 is the Hugoniot for the donor material, line 2 is the reflected Hugoniot for the donor material, line 3 has the slope $\rho_0 U_s^s$ for the sample material, and point 4 is the shock state in the sample material.

In the sample material, the shock velocity is determined using the same method as described for the donor material. To determine the remaining parameters, the impedance matching technique, shown graphically in Fig. 5, was used. The particle velocity in the sample is determined from the intersection of the reflected donor Hugoniot and a line with a slope of $\rho_0 U_s^s$ for the sample. The particle velocity in the sample, U_p^s, can be determined from the following equation, in which the superscript s indicates the sample and d indicates the donor:

$$U_p^s = \frac{-b \pm \sqrt{b^2 - 4ac}}{2a}, \tag{15a}$$

where

$$a = \rho_0^d S^d, \tag{15b}$$

$$b = -(4\rho_0^d S^d U_p^d + \rho_0^d C_0^d + \rho_0^s U_s^s), \tag{15c}$$

$$c = 4\rho_0^d S^d (U_p^d)^2 + 2\rho_0^d C_0^d U_p^d. \tag{15d}$$

The particle velocity could also be approximated by estimating the reflected Hugoniot for the donor as a straight line with a slope of $\rho_0 U_s^d$. Using this estimation, the error associated with the sample particle velocity can be determined from

$$\Delta U_p^s = \sqrt{[\xi \Delta U_s^d]^2 + \left[\left(\frac{2\rho_0^d U_s^d}{(\rho_0^s U_s^s + \rho_0^d U_s^d)}\right)\Delta U_p^d\right]^2 + [-\xi \Delta U_s^s]^2}, \tag{16a}$$

where

$$\xi = \left(\frac{2\rho_0^d \rho_0^s U_s^s U_p^d}{(\rho_0^s U_s^s + \rho_0^d U_s^d)^2}\right). \tag{16b}$$

The pressure in the sample and its associated error can be determined from Eqs. (12) and (14), in which the density, shock velocity, and particle velocity are those associated with the sample material rather than the donor material.

A. Explosive-donor interaction

Using the combination of Baratol, TNT, and Octol pads with copper and aluminum driver plates, shock velocities ranging from 5–7 km/s can be achieved in the metal donor material. This provides a range of input pressures into the samples and enables a reasonable quantification of the Hugoniot in the mid to high pressure range.

Table III presents the measured shock velocity and calculated pressure and particle velocity for all explosive-donor combinations. Experiments JJH8–13 were conducted with a 12.7 mm thick explosive pad in contact with the plane wave lens. It is believed that this is not a large enough distance to achieve a steady detonation wave in the explosive pad, so later experiments utilized an explosive pad that was 25.4 mm thick. These data remain usable, although the pressure is likely below that of the predicted detonation pressure in the explosives.

It can be seen that the experiments are very repeatable. However, the earlier experiments, JJH14–16 and JJH24–26 do not agree as well with the better-calibrated experiments that were performed later. This could be due to the increased number of pins in later experiments (20 vs 9) and the improved tilt correction and statistics associated with the increased number of pins. Additionally, the pins in the early experiments used a thicker piezoelectric crystal (0.5 vs 0.25 mm), which have a longer fall-off time. The pins are placed in close proximity so the shock velocity is measured over a small distance. In the early experiments, several pin records overlapped, making it difficult to distinguish the time when the signal deviates from the baseline, and, subsequently, adding to the uncertainty in the experiment.

1. Equation of state measurements

The measured results (shaded) and calculated values obtained from the gas gun and explosive loading experiments are presented in Table IV. The shock velocity values correspond to those measured based on time of travel through the sample thickness between the input and propagated stress gauges in the gas gun experiments and between piezoelectric pins in explosive loading experiments. Stress profiles recorded by the PVDF gauges in the gas gun experiments provided the magnitude of the stress entering the sample. Figure 6(a) shows examples of stress profiles recorded by the input stress gauge as the shock wave generated upon impact of the flyer on to the driver enters the sample. Figure 6(b) shows the transmitted stress pulses for experiments 0303, 0311, and 0403 following travel through approximately 4 mm thickness of composite material, with corresponding peak pressures of 1.7, 2.9, and 3.6 GPa, respectively. The rise time to peak pressure decreases with increasing stress. The lower pressure experiment (0303) shows a highly dispersed stress wave profile due to wave dispersion, similar to behavior observed by Anderson *et al.* in alumina-filled epoxy.[2] The material tested in experiment 0303 had a lower density than the other samples tested. This point is included for comparison, but is not used when analyzing the data.

The results combining the data obtained from the gas gun and explosive loading experiments are plotted in the

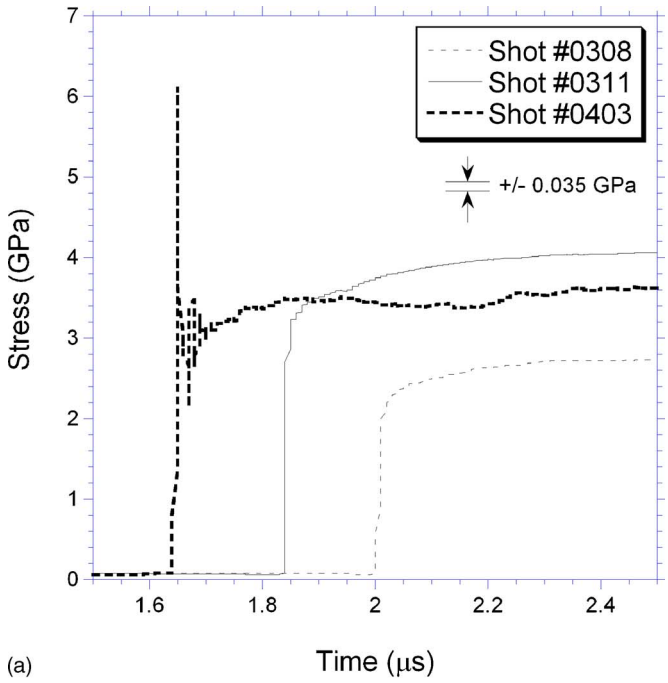

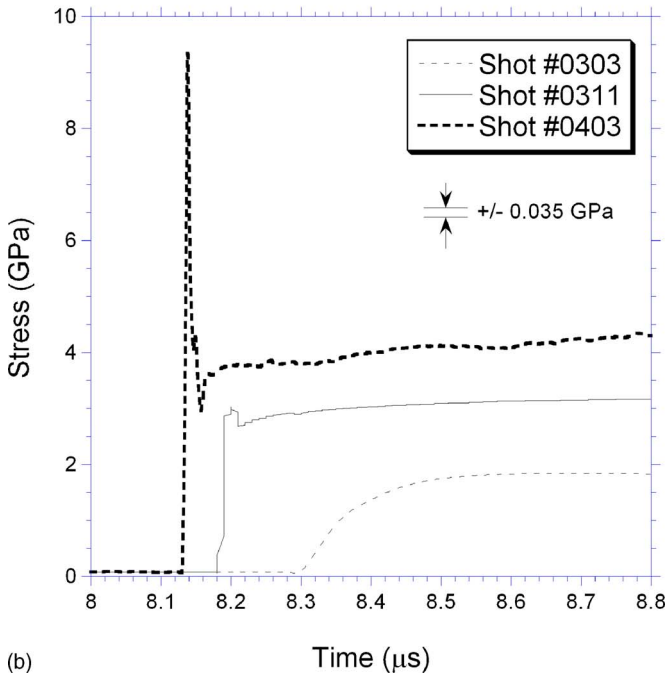

FIG. 6. (Color online) PVDF gauge traces from (a) input gauge and (b) transmitted gauge.

U_s-U_p and P-U_p space, as shown in Figs. 7(a) and 7(b). The line fitted through the data points (except for the datum corresponding to shot 0303, which had a sample of lower density) exhibits a smooth trend without any obvious discontinuities.

The error in the explosive loading experiments, detailed in Table IV, is larger than the ~3% error in stress and 0.2% error in timing measurements in the case of the gas gun experiments. These larger errors could be due to the curvature of the shock wave after it enters the donor. Additionally, the 0.5 mm crystal piezoelectric pins were used in all of these experiments, and deconvolution of the individual pin

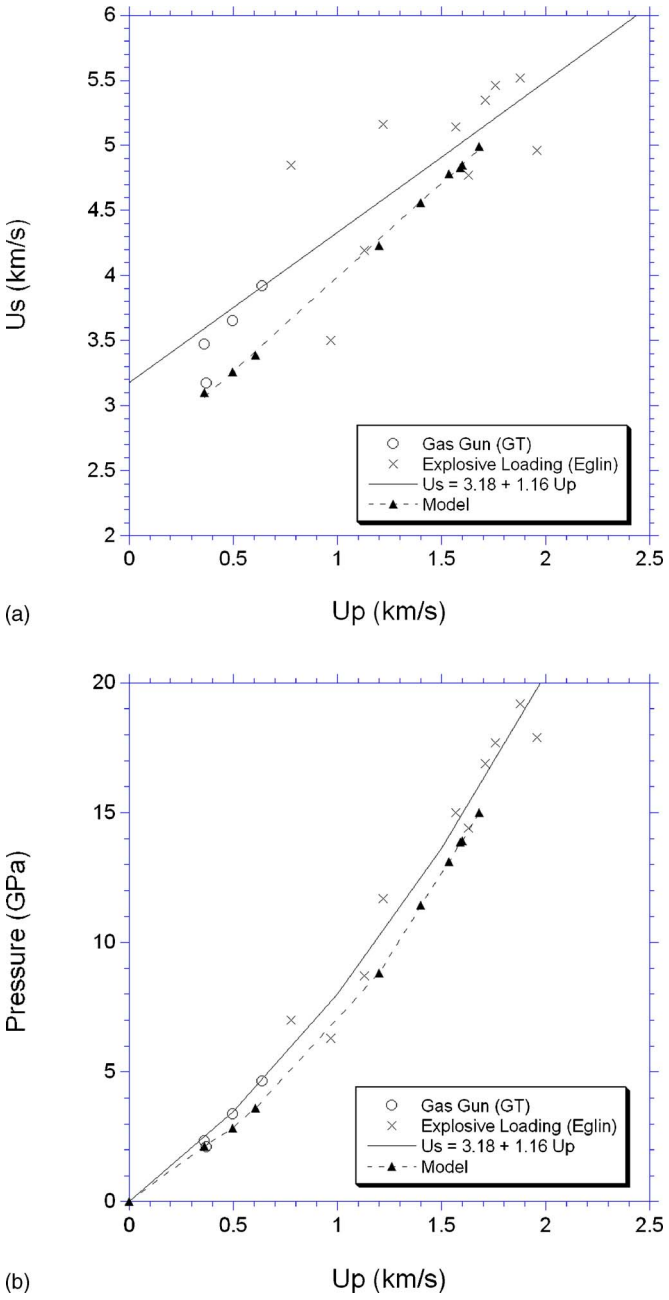

FIG. 7. (Color online) Hugoniot plots based on calculated and measured values obtained from gas gun and explosive loading experiments: (a) pressure vs particle velocity; (b) shock velocity vs particle velocity, in comparison with mesoscale finite-element calculations. The linear fit to this plot defines the dynamic bulk sound speed (3.18 km/s) and the empirical parameter S (1.16).

responses proved to be difficult in several cases. Another source of error, especially for data obtained using a copper donor, is the large impedance mismatch between the copper and composite material, which may translate to larger uncertainty compared to the 6061-T6 Al. In both the gas gun and explosive loading experiments, the errors are associated with measurements of the experimental parameters and are not meant to represent multiple tests at the same input pressure. In the gas gun experiments, these errors are due to the inherent limitations of the measurement devices, and, in the explosive loading experiments, these errors are due to the linear fit to the time-distance data required for determining the shock velocity.

Considering a linear fit to the data shown in the shock velocity versus particle velocity plot in Fig. 7(a), values of the dynamic bulk sound speed, C_0, and empirical parameter, S, were obtained for the Al/Fe_2O_3/epoxy cast cured samples. For these materials, values of C_0 equal to 3.17 km/s and S equal to 1.16 were obtained. The bulk sound speed of the material from ultrasonic measurements is 2.2 km/s,[13] and the values calculated from mass averaging the properties of the components are a C_0 value equal to 4.41 km/s and S equal to 1.38.[11] The curve-fit depicted in Fig. 7(b) is the translation of the linear relationship determined in the U_s-U_p space to P-U_p space. This assumes that the stress measured by the PVDF gauges is equivalent to the hydrodynamic response, which was shown by Deas *et al.*[3] to be true for alumina-epoxy composites tested in a flyer impact configuration with velocities ranging from 190–670 m/s.

Although there is considerable scatter in the data, particularly in the intermediate particle velocity range, the smooth trend exhibited by the data from both sets of experiments, with no apparent discontinuities in the Hugoniot, indicates that there are no chemical or physical changes occurring at pressures up to 19 GPa in the Al/Fe_2O_3/epoxy composite samples containing the large volume fraction of epoxy.

2. Comparison of measured Hugoniot with finite-element model simulations

Shock wave propagation in discrete particles mixtures has been studied at the mesoscale by Benson and co-workers for a range of material systems, e.g., Cu powders,[14,15] HMX,[16] Ti-SiC,[17] and Nb-Si.[18,19] Recently, mesoscopic finite-element models have been developed to enable the study of shock waves in Al/Fe_2O_3/epoxy composite systems.[20] In the aforementioned modeling efforts, thermomechanical responses have been resolved at the level of the microstructure. The following discussion provides a broad overview of the methodology for modeling shock wave propagation in Al/Fe_2O_3/epoxy composite systems; the literature should be consulted for in-depth modeling details.

The shock wave simulations are performed in a 2D multimaterial Eulerian finite-element code developed by Benson.[21] Eulerian formulations are necessary in these calculations due to the severity of deformation (material flow). The governing equations (conservation of mass, momentum, and energy) are solved sequentially using an operator split.[22] Here, the central difference method is used to advance the solution in time during the Lagrangian step. Advection algorithms are used to transport material between cells of the spatially fixed Eulerian mesh during the Eulerian step (solution remap) while time remains constant. Heat generation and heat transfer are included so that thermal and mechanical effects are coupled in the solution. The plane-strain condition is imposed due to the computational demands of fully 3D calculations.

The explicit microstructure of the particle mixtures must be reconstructed for simulation. Discrete sets of particles are

generated from lognormal size distributions that correspond to those measured in actual particle mixtures. Volume fractions of the particle phases and pores in the simulations are matched to those studied in experiments. Particles are located in the domain using a random sequential addition process.[23] A two-point spatial correlation is imposed on the distribution of Al particles; here, a simulated annealing technique is used to evolve the first-nearest-neighbor distributions in the Al phase to that estimated in the actual microstructure. The final result is a 2D rectangular cross section of a particle mixture to be analyzed using finite-element simulation.

Boundary conditions are applied to the domain to achieve nominal 1D shock wave propagation. A velocity boundary condition is imposed on one edge of the domain to generate the shock wave. The boundary conditions for all remaining edges are "rollers" (i.e., normal displacements are constrained to be zero and tangential displacements are unconstrained). The simulations are terminated before the shock front reaches the remote boundary so that wave reflections are avoided.

A set of constitutive models is required to define the stress-strain behavior of each phase. During simulation, the stress response is decomposed into hydrostatic and deviatoric terms, which necessitates the definition of an equation of state (EOS) and strength model for each phase. The Mie-Gruneisen EOS is used to model the hydrostatic response of the Al and epoxy phases, while the Birch Murnaghan EOS (Ref. 24) is used for the hydrostatic response of the Fe_2O_3 phase. The Klepaczko model[25] defines the rate-dependent plastic flow and strain hardening of the Al phase. The Hasan-Boyce model[26] defines the rate-dependent behavior of the epoxy matrix. Since a physically based constitutive stress-strain model is not available for the Fe_2O_3 phase, a simple isotropic elastic-plastic strength model with a small degree of work hardening is adopted.

Results are extracted from the simulations by using simple homogenization techniques to calculate EOS data for the macroscopic mixture. The shock velocity in a simulation is calculated by tracking the position of the shock front with respect to time. The shock pressure is calculated by volume averaging the pressure in a region of the microstructure that is sufficiently far away from both the applied velocity boundary condition and the shock wave front. The particle velocity is known in the simulations; it is imposed (as a boundary condition) to match that measured in an experiment.

The U_s-U_p and P-U_p relations calculated from the model are plotted in Figs. 7(a) and 7(b), respectively. As shown in Fig. 7(a), shock wave velocity calculations agree well with experimental data in the high-velocity regime ($U_P \geq 1.000$ km/s), as differences are less than 8%; differences are somewhat larger (capped at 14%) in the low-velocity regime ($U_P < 1.000$ km/s). This trend is in agreement with prior observations by Benson[15] for Cu powders, where larger deviations in the shock wave speed calculations were observed at lower particle velocities. As shown in Fig. 7(b), stationary pressure calculations show good agreement with experimental data in the low-velocity regime, as differences are less than 7%; differences are somewhat larger (capped at 12%) in the high-velocity regime. Despite discrepancies in the U_s-U_p relation, it is encouraging to observe a linear dependence between the shock wave velocity and particle velocity, as such relations describe many material systems. The deviations in calculations of U_S and P_{st} are tentatively attributed to the 2D approximation of the microstructure.

IV. CONCLUSIONS

Equation of state experiments in the 2–19 GPa pressure range were conducted on Al/Fe_2O_3/epoxy composites. Lower pressure experiments were performed using an 80 mm diameter single-stage light-gas gun. The input and propagated pressures, as well as the shock velocity in the material were recorded using PVDF piezoelectric gauges. In order to achieve higher pressures, explosive loading of the samples was conducted using TNT/Octol plane wave lenses with Baratol, TNT, and Octol pads and aluminum, copper, and PMMA donor plates to vary the input pressure. Shock velocity measurements were obtained using piezoelectric pins in the sample and in donor materials, in order to perform impedance matching to determine the remaining properties in the sample. The data from both sets of experiments illustrate a continuous trend with no evidence of any physical or chemical change occurring in the Al/Fe_2O_3/epoxy composites at pressures up to 19 GPa. It is satisfying that the gas gun data and the explosively derived data are comparable. Finally, mesoscale finite-element modeling results show good agreement with experimental data.

ACKNOWLEDGMENTS

The authors would like to thank the MNME Processing and Dynamics Chamber teams. Several of the authors (L.F., N.N.T., R.A.A., and D.L.M.) acknowledge the funding obtained through AFOSR/MURI Grant No. F49620-02–1-0382 and the Graduate Research Internship Support (for L.F.) provided by AFRL/MNME, Department of the Air Force Contract No. F08630-03-C-001. Funding for R.D.D. was provided by AFRL/MNME, Department of the Air Force Contract No. FA8651-05-C-0027. J.L.J. and J.R.F. would like to acknowledge AFRL/MNME, AFRL/MNMF, and AFOSR (PM: Dr. Victor Giurgiutiu) for supporting this research. Opinions, interpretations, conclusions, and recommendations are those of the authors and not necessarily endorsed by the United States Air Force.

[1] D. E. Munson, R. R. Boade, and K. W. Schuler, J. Appl. Phys. **49**, 4797 (1978).
[2] M. U. Anderson, R. E. Setchell, and D. E. Cox, *Shock Compression and Release Properties of Alumina-Filled Epoxy in Shock Compression of Condensed Matter - 2003*, Portland, OR (American Institute of Physics, Melville, NY, 2004).
[3] D. Deas *et al.*, *The Shock Hugoniot of Two Alumina-Epoxy Composites in Shock Compression of Condensed Matter - 2003*, Portland, OR (American Institute of Physics, Melville, NY, 2004).
[4] J. G. T. Holman, R. A. Graham, and M. U. Anderson, *Shock Response of Porous* $2Al+Fe_2O_3$ *Powder Mixtures* (American Institute of Physics, New York, 1994).
[5] R. A. Austin, D. L. McDowell, and D. J. Benson, Model. Simul. Mater. Sci. Eng. **14**, 537 (2006).
[6] F. Bauer, United States Patent 4684337 (1987).
[7] R. D. Dick, "Shock Wave Compression of Benzene, Carbon Disulfide,

Carbon Tetrachloride, and Liquid Nitrogen," thesis, Arizona State University (1968), p. 103.
[8]Y. Bar-Shalom, X. R. Li, and T. Kirubarajan, *Estimation with Applications to Tracking and Navigation* (Wiley, New York, 2001).
[9]P. E. Gill, W. Murray, and M. H. Wright, *Practical Optimization* (Academic, London, 1981).
[10]W. H. Press *et al.*, *Numerical Recipes in Fortran 77: The Art of Scientific Computing* (Cambridge University Press, Cambridge, 1992).
[11]*Shock Hugoniot Data*, edited by S. P. Marsh (University of California Press, Berkeley, 1980).
[12]M. A. Meyers, *Dynamic Behavior of Materials* (Wiley & Sons, New York, 1994), p. 668.
[13]N. N. Thadhani *et al.*, "Chemical Reaction and Mechanical Behavior of Multifunctional Structural Energetic Materials," in *Shock Compression of Condensed Matter - 2003*, Portland, OR (American Institute of Physics, Melville, NY, 2003).
[14]D. J. Benson, Model. Simul. Mater. Sci. Eng. **2**, 535 (1994).
[15]D. J. Benson, Wave Motion **21**, 85 (1995).
[16]D. J. Benson and P. Conley, Model. Simul. Mater. Sci. Eng. **7**, 333 (1999).
[17]D. J. Benson, W. Tong, and G. Ravichandran, Model. Simul. Mater. Sci. Eng. **3**, 771 (1995).
[18]I. P. H. Do and D. J. Benson, Int. J. Comput. Eng. Sci. **1**, 61 (2000).
[19]I. P. H. Do and D. J. Benson, Int. J. Plast. **17**, 641 (2001).
[20]R. A. Austin, D. L. McDowell, and D. J. Benson, Model. Simul. Mater. Sci. Eng. **14**, 537 (2006).
[21]D. J. Benson, Comput. Mech. **15**, 558 (1995).
[22]D. J. Benson, Comput. Methods Appl. Mech. Eng. **99**, 235 (1992).
[23]S. Torquato, Appl. Mech. Rev. **44**, 37 (1991).
[24]F. D. Murnaghan, Am. J. Math. **59**, 235 (1937).
[25]J. R. Klepaczko, T. Sasaki, and T. Kurokawa, Trans. Jpn. Soc. Aeronaut. Space Sci. **36**, 170 (1993).
[26]O. A. Hasan and M. C. Boyce, Polym. Eng. Sci. **35**, 331 (1995).